Antibiotic Resistance Peptides: Interaction of Peptides Conferring Macrolide and Ketolide Resistance with *Staphylococcus aureus* Ribosomes. Conformation of Bound Peptides As Determined by Transferred NOE Experiments†

Laurent Verdier,‡,§ Josyane Gharbi-Benarous,‡,§ Gildas Bertho,‡ Pascale Mauvais,|| and Jean-Pierre Girault*,‡

Laboratoire de Chimie et Biochimie Pharmacologiques et Toxicologiques, Université René Descartes-Paris V, UMR 8601 CNRS, 45 rue des Saint-Pères, 75270 Paris Cedex 06, Université Denis Diderot-Paris VII, UFR Chimie, 2 Place Jussieu, F-75251 Paris Cedex 05, and Aventis, 102 route de Noisy, 93235 Romainville Cedex, France

Received June 25, 2001

ABSTRACT: Two antibiotic resistance peptides, the E-peptide (MRLFV) and the K-peptide (MRFFV) conferring macrolide and ketolide resistance, respectively, were studied in the complex state with bacterial *Staphylococcus aureus* ribosomes. Interactions of antibiotic resistance peptides with ribosomes were investigated using two-dimensional transferred nuclear Overhauser effect spectroscopy (TRNOESY), suggesting that the peptide−ribosome interaction was associated with the low-affinity binding level. K-Peptide displayed a significantly better response in TRNOEs NMR experiments, in agreement with a better overall antibiotic activity of ketolides. This difference highlights a mimetic effect displayed by the E- and K-peptides. This study shows that conformation plays an essential role for the affinity binding site and, thus, for the resistance mechanism. Specific conformations were preferred in the bound state; their superimposition exhibited a similar cyclic peptidyl chain, while the side chain region varies. The F4 phenyl moiety in E-peptide has moved out of the turn region compared to its folding in the ketolide resistance peptide. In the K-peptide binding surface, the F4 aromatic chain is maintained by stacking with the guanidyl group of the R2 residue providing a particular hydrophobic and globular fragment, which may be important for the ketolide resistance peptide mode of action. Additionally, T_2 (CPMG) measurements were used to characterize equilibrium binding of antibiotic resistance peptides to bacterial ribosomes. The results bring to the fore E- and K-peptide competition with antibiotics for binding to the ribosomes. Their specific interaction and their competitive effects reveal a novel aspect of interaction of resistance peptides with ribosomes and suggest new insights about their mode of action. The resistance mechanism may imply two steps, a competitive effect of the resistance peptide for the macrolide (or ketolide) binding site followed by a "bottle brush" effect in which the drug and the peptide are driven out their binding site on the ribosome.

Macrolides and ketolides are important antibacterial antibiotics. The emergence of bacteria resistant to existing antibacterial agents, including macrolide antibiotics, has accelerated the search for newer and more effective antibacterial agents (*1*). The development of the structure−activity relationships is driving the resurgence of interest in macrolides. The new class of antibiotics called ketolides is endowed with remarkable antibacterial activity against macrolide-resistant strains. Telithromycin was selected to be the ketolide candidate with a favorable pharmacodynamic profile for the clinical trials, to be put on the market. This class of macrolides, termed "ketolides", demonstrated significantly improved activity against MLS (macrolide, lincosamide, and streptogramin B) inducibly resistant organisms (*2*−*5*). These agents, such as the ketolide telithromycin, have higher in vitro potencies than macrolides, and in vivo infection model results were quite promising (*6*). Telithromycin has been shown to be active against a variety of bacteria, including macrolide-resistant bacteria and mycobacteria and also to exhibit good intracellular penetration (*1*). The mechanism of action of ketolides has been observed to be similar to that of the macrolides by means of binding to the 50S ribosomal subunit (*7*−*9*) and the subsequent inhibition of bacterial protein synthesis (*10*, *11*). There appears to be two stages to this binding: a weak interaction which can be detected by NMR spectroscopy (*12*) and a stronger interaction observed by different methods (*7*−*9*). The weak binding of antibiotics to *Escherichia coli*, erythromycin-sensitive and -resistant strains of *Streptococcus pneumoniae*, and *Staphylococcus aureus* ribosomes (*13*) has been characterized extensively by line broadening and transferred NOESY (TRNOESY)[1] experiments and was only observed with the antibiotics belonging to the MLS_B classes which have exhibited good activity (*12*, *14*, *15*), the 14- and 16-membered macrolides (*12*, *16*−*18*), the new class of antibiotics called ketolides

† This work was supported by grants from the Romainville Research Center of Medicinal Chemistry of Hoechst Marion Roussel (Aventis).

* To whom correspondence should be addressed. Telephone: 01 42 86 21 80. Fax: 01 42 86 83 87. E-mail: girault j@biomedicale.univ-paris5.fr.

‡ Université René Descartes-Paris V.

§ Université Denis Diderot-Paris VII.

|| Aventis.

10.1021/bi011319e CCC: $22.00
Published on Web 03/08/2002

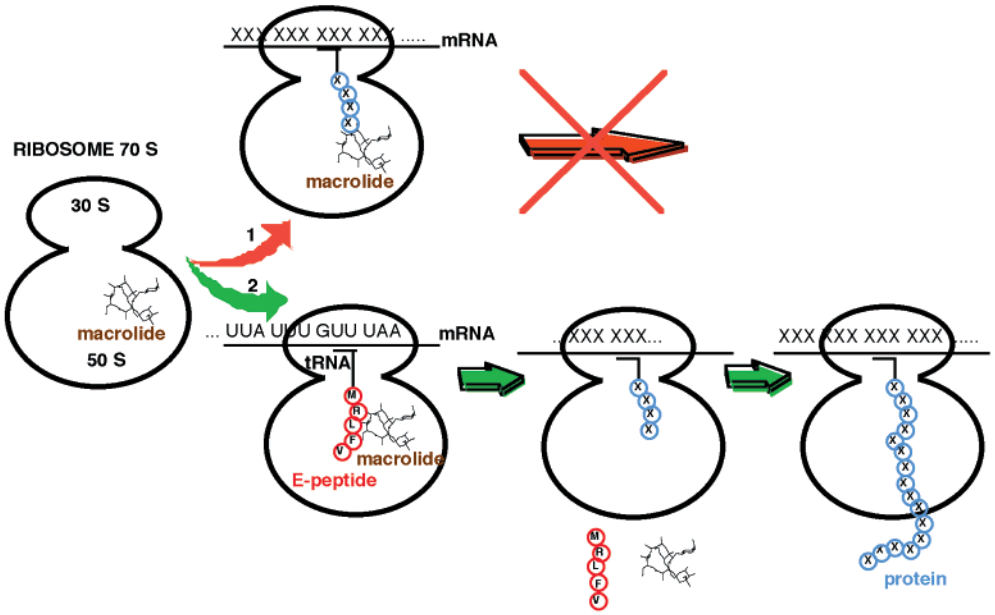

FIGURE 1: Model of action of macrolide resistance peptides (*28*). (1) Binding of a macrolide to the 50S ribosomal subunit hinders growth of the nascent peptide chain in the early rounds of protein synthesis and then exerts antibiotic activity in inhibiting protein biosynthesis in the elongation step. (2) Translation of a macrolide resistance peptide "cleans" the ribosome from antibiotic. If an antibiotic-free ribosome initiates synthesis of a cellular protein and polymerizes the first two to five amino acids, it will become "immune" to an antibiotic until the completion of polypeptide synthesis because macrolides cannot bind to ribosomes containing long nascent peptides.

(*1*, *19*, *20*), and the lincosamides (*21*). Compounds which are not able to take part in a weak binding interaction with bacterial ribosomes do not exert any antibiotic activity (*22*), which was also observed by Barber et al. (*14*). Thus, the weak binding site seems to be a necessary step for the strong interaction (*23*, *24*). This weak binding observed by TRNOE experiments could be involved in the first step of recognition and selection of antibiotics by the ribosomal machinery.

Nevertheless, the clinical use of antibiotics is significantly hampered by the growing number of resistant strains (*25*). Different mechanisms of resistance have been described (*25*, *26*): (a) mechanisms affecting accumulation of the drug in the cell, (b) mechanisms involving modification of the drug target, and, finally, (c) mechanisms based on the modification of the drug. A novel mechanism (Figure 1), a hybrid of the latter two which is based on interaction of specific short peptides with the ribosome, has been proposed recently (*27*, *28*). The antibiotics sterically hinder growth of the nascent peptide chain (*29*) and may promote dissociation of peptidyl-tRNA (*30*, *31*). Despite this, a nascent pentapeptide can interact directly with the drug and, so, displaces the antibiotic from the ribosome. These peptides act probably as a "bottle brush" that "cleans" the ribosome from the bound antibiotic (*28*). The discovery of this resistance mechanism came from an observation that overexpression of a short segment of *E. coli* 23S rRNA (positions 1235−1268) rendered cells resistant to erythromycin. It is unclear yet whether E-peptide is expressed naturally, because the peptide minigene ribosome-binding site is sequestered in the rRNA secondary structure (*27*). Mutational and biochemical analyses demonstrated that resistance is caused by translation of a pentapeptide open reading frame (ORF) encoded in *E. coli* 23S rRNA and is mediated by interaction of the newly translated pentapeptide with the ribosome. The rRNA-encoded pentapeptide is not normally expressed because the Shine-Dalgarno region of the peptide ORF is sequestered in the 23S rRNA secondary structure. However, peptide expression can be activated by site-specific fragmentation of rRNA or by rRNA mutations that increase accessibility of the Shine-Dalgarno region of the E-peptide ORF (*32*). The peptide enters the site of its action cotranslationally and acts in cis, affecting properties of only that ribosome on which it has been translated (*33*). Analysis of more than 70 pentapeptides that can confer resistance to erythromycin (E-peptides) revealed a consensus sequence (MXLXV) which could be recognized in the majority of E-peptides and was especially pronounced in the most active E-peptides that could confer very high levels of erythromycin resistance (*33*). Analysis of ketolide resistance clones revealed a sequence (MRFFV) which is one of the best that confers resistance to the ketolide (K-peptide). Different peptides confer resistance to different macrolides. The E-peptide MRLFV rendered cells resistant to high concentrations of erythromycin, but not ketolide; conversely, expression of the K-peptide MRFFV afforded a high level of ketolide resistance but did not protect the cell from high erythromycin concentrations. The nature of the expressed peptide determines the macrolide to which the cell will become resistant. The size of the peptide (three to six amino acids) and its amino acid sequence are essential for its functions. Moreover, these peptides affect sensitivity to only macrolide (or ketolide) antibiotics. Expression of the E-peptide increased cell resistance not only to erythromycin but also to other macrolide antibiotics, whereas sensitivity

[1] Abbreviations: E-peptide, pentapeptide conferring erythromycin resistance; K-peptide, pentapeptide conferring ketolide resistance; NOESY, nuclear Overhauser effect spectroscopy; ROESY, rotating frame Overhauser enhancement spectroscopy; TOCSY, total correlation spectroscopy; COSY, correlation spectroscopy; HSQC, heteronuclear single-quantum correlation; INEPT, insensitive nuclei enhanced by polarization transfer; WATERGATE, water suppression by gradient-tailored excitation.

to chloramphenicol and clindamycin was not affected (*33*).

We report here the study of the interaction with *S. aureus* ribosomes of two pentapeptides, the E-peptide (MRLFV) and the K-peptide (MRFFV), conferring macrolide and ketolide resistance, respectively. Mankin and co-workers suggested that the biosynthesized pentapeptides in the elongation step do not just passively occupy the drug binding site but actively displace the antibiotic from the ribosome (*28*). This model does not require specific association of the resistance peptide with the ribosome. The ribosome may constrain the synthesized peptide in a conformation competent for specific interaction with the antibiotic. Such interaction may reduce the affinity of the drug for its binding site on the ribosome, and it can be ejected together with the completed peptide (*28*). However, this resistance could also be caused by specific interaction of the translated short peptide with the ribosome (*33*, *34*). In this article, we will try to shed light on the mechanism of action of antibiotic resistance peptides and to observe if it could be similar to that of macrolides and ketolides by means of binding to the 50S ribosomal subunit. In this study, we have utilized NMR spectroscopy to directly observe and characterize antibiotic resistance peptide binding to bacterial ribosomes. This paper reports direct measurements of the dissociation equilibrium constants (K_D) for the peptide−ribosome complex by the T_2 (CPMG) method (*35*, *36*). Furthermore, competitive antibiotic displacement was also tested in a series of T_2 CPMG measurements to compare the inhibition behavior of E- and K-peptides in solution containing the antibiotic and ribosome.

MATERIALS AND METHODS

Purification of Ribosomes. The *S. aureus* O11UC4 70S ribosomes were prepared at Hoechst Marion Roussel (HMR) as described by Umejawa (*37*) and Swenden (*38*).

Sample Preparation and NMR Spectroscopy. The three peptides (the E-peptide MRLFV, the K-peptide MRFFV, and the control peptide MDVEQ) were synthesized by NEOSYSTEM (Strasbourg, France), and the purity (99%) was checked by HPLC analysis (E-peptide MW = 665 g/mol and K-peptide MW = 699 g/mol). The peptides were dissolved in an aqueous NaH_2PO_4/Na_2HPO_4 buffer (0.05 M), with KCl (0.2 M) at a physiological apparent pH 7.6, and we could attain concentrations of 2.0 mM. They were placed into 5 mm NMR tubes to obtain 0.5 mL of 90% buffer/10% D_2O samples. Crystals of 3-(trimethylsilyl)propionic-2,2,3,3-d_4 acid (sodium salt) were included in all samples to provide reference signals, and 0.02% NaN_3 was added to inhibit microbial growth. The experiments were carried out for all samples at 500 MHz for ^1H, at 278, 283, and 293 K, on a Bruker AMX 500 spectrometer equipped with a Silicon Graphics workstation. Phase-sensitive two-dimensional (2D) TOCSY, NOESY, and ROESY spectra were recorded by standard techniques using the time-proportional phase incrementation mode (States−TPPI). Suppression of intense solvent resonances was achieved by use of the WATERGATE sequence (*39*). The 2D TOCSY spectra were recorded with data matrixes of 2K × 256 points and processed using shifted sine bell squared window functions with zero filling in F_1 to 2K × 1K. The mixing times were 30 and 80 ms. The 2D phase-sensitive COSY spectra with gradient selection (*40*) were recorded with data matrixes of 2K × 256 points using the States−TPPI mode. The 2D phase-sensitive ^1H NOESY experiments were performed using different mixing times from 400 to 1000 ms. For ROESY experiments, a spin lock of 200−400 ms was used. FIDs were acquired over 5555 Hz into a 2K point data block for 256 incremental values of the evolution time and a relaxation delay of 2 s. The inverse correlation ($^1H-^{13}C$) PFG-HMQC experiments (*41*) were carried out using a transfer delay of 3.5 ms, with 256 experiments of 2048 data points, and 400 scans per experiment. One millisecond half-sinusoid gradients of 40, 40, and 20 G/cm were used to select protons attached to carbon. We performed a better water suppression by a presaturation (65 dB) during the relaxation delay. To decrease the experimental time, we have performed phase-sensitive HSQC using echo/anti-echo gradient selection with decoupling during acquisition (*42*). The 2D $^1H-^{13}C$ correlations were obtained via double-INEPT transfer using a TRIM pulse (200 μs at 5 dB). The spectra were recorded with 256 experiments of 2048 data points, with 48 scans per experiment. One millisecond half-sinusoid echo/anti-echo gradients of 80 and 20 G/cm with a recovery delay of 200 μs were used. To select protons attached to carbon, a delay of 1.78 ms was optimum for C−H one-bond couplings (delay = $^1/_4{}^1J_{C-H}$ delay). This technique is optimized to obtain $C_\alpha-H_\alpha$ correlations with a sensitivity enhancement.

Transferred Nuclear Overhauser Effect. The method of transferred NOE NMR spectroscopy (TRNOE) (*43*, *44*) allows observation of a bound ligand as it transfers cross relaxation to the free state, if the rate of chemical exchange is faster than the T_1 longitudinal relaxation rate of the free ligand. In addition, the contribution of the bound state must be greater than the contribution of the free state, i.e., $|X_b\sigma^b| \gg |X_f\sigma^f|$, where X_b is the ligand mole fraction that is bound and X_f is the ligand mole fraction that is free ($X_b + X_f = 1$). This condition is valid because the cross relaxation of the bound ligand (σ^b) which has a very large molecular weight is much greater than that for the free ligand (σ^f) in aqueous solution. The bound and free states exist in two different regimes, namely, $\omega\tau_c < 1$ (free) and $\omega\tau_c > 1$ (bound). Thus, the cross-relaxation rates of the two small peptides (E-peptide MW = 665 g/mol and K-peptide MW = 699 g/mol) in the free and bound state are of opposite sign, such as NOEs in the free state that are positive and those in the bound state that are negative.

The 2D phase-sensitive States−TPPI method, ^1H TR-NOESY experiments in buffered solution were performed using different mixing time of 50−150 ms. FIDs were acquired (96 scans) over 5555 Hz into a 2K data block for 256 incremental values of the evolution time and a relaxation delay of 2 s. Transferred NOE effects from peptide−ribosome interactions could be observed with a ligand/ribosome ratio of 5000 at 293 K. A *S. aureus* O11UC4 70S ribosome concentration of 0.4 μM is appropriate because it gives a significant increase in the line width of E- and K-peptide. Suppression of intense solvent resonances was achieved by use of the WATERGATE sequence.

T_2 CPMG Competitive Experiments. The Carr−Purcell−Meiboom−Gill (CPMG) (*45*) spin-echo decay rate was used to estimate the rate of dissociation of the antibiotic−ribosome complexes. The observed relaxation rate ($1/T_{2obs}$) equals the

weighted average of both the relaxation rates of the free ($1/T_{2f}$) and bound [$1/(T_{2b} + \tau_b)$] ligand (*46*)

$$\frac{1}{T_{2obs}} = \frac{X_f}{T_{2f}} + \frac{X_b}{T_{2b} + \tau_b} \quad (1)$$

where T_{2b} is the transversal relaxation time, τ_b is the exchange lifetime of the bound antibiotics, and T_{2f} equaled the observed antibiotic T_2 in buffer. The determination of the competitive dissociation equilibrium constant $K_{D(I)}$ was conducted according to a previously described procedure (*13*). The inhibitor peptide is added gradually to a solution containing 1 mM antibiotic (roxithromycin or telithromycin) and 0.2 μM *S. aureus* ribosomes at molar ratios (peptide/ribosome) ranging from 2500 to 9000. Competitive titrations were performed by repeatedly adding in the concentration range of a few millimolar the competitive peptide (E- or K-peptide) to the existing NMR sample at 293 K. The relaxation behavior of the known ligand (**L**, antibiotics in our case) which binds to a macromolecule (**R**, the ribosome) as a function of a competitive inhibitor (**I**, the peptides) concentration is described (*46*) as

$$\frac{[R]_T}{\frac{1}{T_{2obs}} - \frac{1}{T_{2f}}} = \frac{(T_{2b} + \tau_b)K_{D(L)}}{K_{D(I)}}[I] + \left[\frac{1}{(T_{2b} + \tau_b)} - \frac{1}{T_{2f}}\right][K_{D(L)} + [L]]$$

where [L] and [I] are the total concentrations of the ligand (**L**) and the competing ligand (**I**) (with the binding site concentration, $[R]_T$, constant), respectively, and $K_{D(L)}$ and $K_{D(I)}$ are the dissociation constants of the initial ligand (**L**) and the competing ligand (**I**), respectively. A straight line is obtained from the plot of $[R]_T/(1/T_{2obs} - 1/T_{2f})$ versus [I]. Since the value of $T_{2b} + \tau_b$ was previously determined for the ligand (**L**) in the absence of the competing ligand (**I**), the slope directly provides the value for the $K_{D(L)}/K_{D(I)}$ ratio (Figure 2).

Spin−spin relaxation (T_2) measurements (*35*, *47*) were taken using the CPMG pulse sequence. A nonselective 90° pulse ($t_{90} \sim 30$ μs) was first applied to excite the sample followed by multiple nonselective 180° refocusing pulses ($t_{180} \sim 60$ μs) to generate the echo train. τ_{cp} is the time between refocusing 180° pulses in the CPMG pulse train, and it was fixed at 2 ms. The relaxation delay between successive echo sequences ($d_1 = 4$ s) was more than 4 times greater than T_1 to ensure sample equilibrium. Relaxation data were collected for an interval spanning at least 2−3 times the T_2 decay constant. The data (after 12 experiments) were plotted as a function of echo evolution time and fitted to a single exponential using a nonlinear least-squares fitting program. T_2 values are reported as time constants of these exponentials.

NMR Structure Determination. All structural calculations were run on a Silicon Graphics (SGI) workstation. The correct L-amino acid peptide sequences were built using Insight II/Discover (Biosym Technologies, San Diego, CA). All calculations were performed using the CVFF force field (*48*). In the description of the Coulombic interaction, for implicitly taking into account the solvent, the relative permittivity was distance-dependent ($\epsilon = 4r$). NOE-derived distances [strong (s), 2−3 Å; medium (m), 2−4 Å; and weak (w), 2−5 Å] were used as input constraints for the Discover program. Modifications were made to ensure a trans (180°) peptide bond (ω_i) ($C\alpha_{i-1}-C'_{i-1}-N_i-C\alpha_i$). Starting from an extended template structure, containing a protonated C-terminus to eliminate the electrostatic interaction between NH_3^+ and CO_2^-, we performed 5000 energy minimization steps. After an equilibration period of 6 ps, a 10 ps MD run was performed at 300 K followed by 100 ps of molecular dynamics at 800 K, cooling to 300 K in 50 K steps, and finished by 90 ps of MD at 300 K. The trajectory was sampled every picosecond, and the remaining structures were then minimized by molecular mechanics and stored. The dihedral angles do not show large variations except for the first picoseconds at high temperatures (Figure 9 in the Supporting Information). The final conformers with the lowest energies were then further minimized to a gradient of less than 0.01 kcal/mol to obtain their energies with a higher accuracy. Thus, we obtained 200 structures by run. Distances including methyl protons and CH_2 protons were referred to a pseudoatom, located at the mass center of three or two protons.

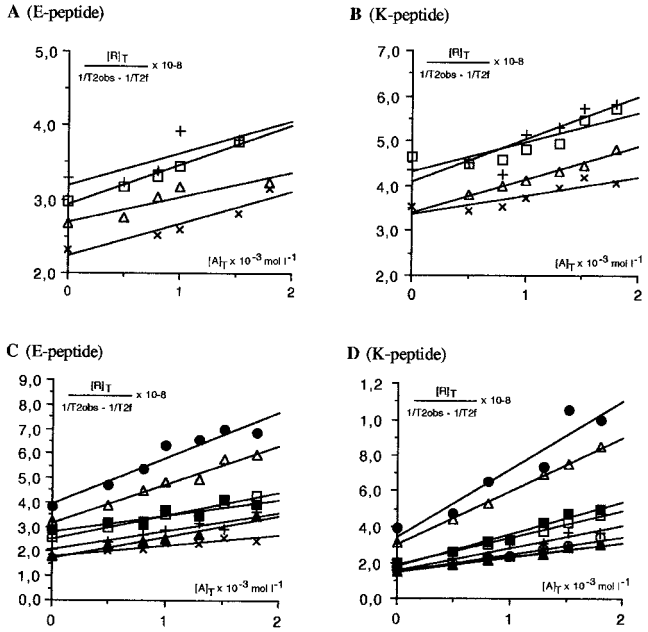

FIGURE 2: Competitive titration plots with *S. aureus* ribosomes (0.2 μM) for the macrolide roxithromycin [(+) 10-Me, (×) 6-Me, (□) 3′-N(Me)$_2$, and (△) 3″-Me] with (A) E-peptide and (B) K-peptide, according to eq 2. Competitive titration plots with *S. aureus* ribosomes (0.2 μM) for the ketolide telithromycin [(+) 10-Me, (×) 6-Me, (□) 3′-N(Me)$_2$, (△) 23, (●) 21, (○) 6-OMe, (▲) 12-Me, and (■) 2-Me] with (C) E-peptide and (D) K-peptide.

RESULTS

Interactions of Antibiotic Resistance Peptides with S. aureus Ribosomes. Upon addition of *S. aureus* ribosomes, the resonances of the K-peptide in a buffer phosphate solution showed a pronounced line broadening in the one-dimensional (1D) proton NMR spectra, indicating its interaction with the ribosomes. Interestingly, the lines corresponding to the E-peptide showed the same effect. The experiments were performed in an aqueous NaD_2PO_4/Na_2DPO_4 buffer (0.05 M) with KCl (0.2 M) at an apparent physiological pH of

7.6. The line broadening of the two peptides is proportional to the amount of ribosome. Physical parameters of crucial importance for chemical exchange such as temperature, substrate/ligand ratio, and *S. aureus* ribosomal concentration have to be optimized (*12*). A low ribosomal concentration (0.4 μM) with a larger fraction of ligand (2 mM) causes half-line broadening of the peptide signals as well as clearly observable TRNOE cross-peaks. If one assumes that the correlation time of the interproton vector motion (τ_c) increases in proportion to the molecular mass of the complex, the TRNOEs would be observable even for a large excess of ligand (*49*). Here, with a ligand/ribosome ratio of 5000, transferred NOE effects from resistance peptide−ribosome interactions can be observed. This result suggested that chemical exchange for antibiotic resistance peptides is similar than for previously studied macrolides (e.g., 5000/1 ratio for 14-membered macrolides) (*12, 18, 22*). A more pronounced broadening was observed for the K-peptide than for the E-peptide, even if the same peptide/ribosome ratio was used. Moreover, the K-peptide's TRNOE cross-peaks are more intense despite a mixing time that is 3 time shorter. These results show that the K-peptide displayed a higher affinity for weak *S. aureus* ribosomal interaction than the other tested E-peptide. Evidence for ribosome−peptide interactions can be seen in the binding-induced line broadening in the NMR spectra of the E- and K-peptides, and the binding affinity can be evaluated by the T_2 (CPMG) method.

Several mechanisms can cause antibiotic relaxation enhancement upon binding to the ribosome. Two experiments should indicate that the relaxation enhancement is caused by the binding of the antibiotic resistance peptides to the ribosome in the binding site, and not by a viscosity increase or nonspecific binding (*50*). (i) One experimental way to distinguish here between specific effects of peptides binding to their targets and nonspecific interactions between small molecules and macromolecular complexes was to use, in control experiments, the MDVEQ peptide in place of the E-peptide (MRLFV) and the K-peptide (MRFFV). This peptide did not conform to a general MRXFV consensus sequence as the previously selected antibiotic resistance E- and K-peptides did. As a control, all strains were not transformed with the plasmid encoding the MDVEQ peptide (*27*). The addition of *S. aureus* ribosomes (0.4 μM) to the MDVEQ peptide (2 mM) results in the absence of broadening of all the lines in the control spectrum and a blank TRNOESY spectrum. It was clear from these data that the E-peptide (MRLFV) and the K-peptide (MRFFV) bound weakly to bacterial ribosomes in a manner similar to that of macrolide and ketolide groups, as indicated by selective line broadening in the ^{1}H NMR spectra and a positive response in the TRNOESY spectra. (ii) The effect observed in the NMR relaxation of an antibiotic induced by binding interaction with ribosomes is specific when competitive antibiotic displacement is observed (*46, 50*) in a series of measurements in which the inhibitor peptide is added gradually to a solution containing antibiotic and ribosome (Figure 2). The observed transverse relaxation time T_2 increases upon addition of the peptides. The plots of T_{2obs} versus inhibitor (E- or K-peptide) concentration, keeping the antibiotic and the ribosome concentration constant, clearly indicate that the line broadening is caused by the binding of the peptides to the ribosome. A straight line is obtained in accordance with eq 2 (Figure 2). The results of competitive experiments indicate an allosteric effect between the peptides and the antibiotics. The binding domain of the E-peptide and the binding domain of the K-peptide partially overlap the site of the weak antibiotic−ribosome interaction.

Competition between the Antibiotic and Antibiotic Resistance Peptides to S. aureus Ribosomes. With the increasing E- and K-peptide concentration in the sample containing either macrolide roxithromycin or ketolide telithromycin, the antibiotic protons relaxed more slowly (Figure 2). Enhancement of the transverse relaxation time and the linearity of the plots illustrate the competition between the E- and K-peptides and the antibiotics and the *S. aureus* bacterial ribosomes according to eq 1. $K_{D(I)}/K_{D(L)}$ values were estimated (±10%) from the titration plots. Straight lines are obtained from the plot of $[R]_T/(1/T_{2obs} - 1/T_{2f})$ versus [I]. Figure 2 shows titration plots of the observed selective T_{2obs} values of the 10-Me, 6-Me, 3′-N(Me)$_2$, and 3″-Me groups of roxithromycin and the T_{2obs} values of the 10-Me, 6-Me, 3′-N(Me)$_2$, and 23-, 21-, and 6-OMe groups of telithromycin, with the E-peptide (Figure 2A,C) and the K-peptide (Figure 2B,D), respectively. The value of $T_{2b} + \tau_b$ has been determined from the slope of the titration plots without inhibitor and was in the range of 2−6 μs for roxithromycin and 4−10 μs for telithromycin. Thus, the slopes obtained in Figure 2 directly provide the value of $K_{D(L)}/K_{D(I)}$ [$K_{D(roxithromycin)}/K_{D(E-peptide)} \approx 1.1$, $K_{D(telithromycin)}/K_{D(E-peptide)} \approx 1.4$, $K_{D(roxithromycin)}/K_{D(K-peptide)} \approx 1.7$, and $K_{D(telithromycin)}/K_{D(K-peptide)} \approx 2.5$]. The E-peptide (MRLFV) and K-peptide (MRFFV) are competitive inhibitors of both macrolide (roxithromycin) and ketolide (telithromycin) for the weak binding antibiotic 50S ribosomal domain. These results suggest that the E- and K-peptide exhibited a higher affinity for weak interaction with the *S. aureus* ketolide ribosomal domain than with the macrolide ribosomal domain (30 and 50%, respectively). On the other hand, the K-peptide has more affinity than the E-peptide tested against *S. aureus* strains at the roxithromycin and telithromycin ribosomal domain (55 and 80%, respectively).

STRUCTURAL DATA

Assignment of Peptide Resonances. TOCSY, COSY, NOESY, and ROESY cross-peak connectivities in the spectra of the E- and K-peptides were used to identify the spin systems of residues. (^{1}H−^{13}C) PFG-HMQC and HSQC experiments have allowed us to assign the resonances without ambiguity. Sequential assignments were used in the case of the K-peptide to differentiate the two phenylalanines F3 and F4. At 500 MHz, TOCSY and COSY spectra were well-resolved but the NOESY spectra generate lower NOE cross-peaks at 500 MHz even with very long NOE mixing times (400−1000 ms). This fact seems to indicate that these peptides do not adopt any favored structures at all, being free in solution. Assignments in H_2O and D_2O obtained at 293 K were reported in Tables 1 and 2 for the E-peptide (MRLFV) and the K-peptide (MRFFV), respectively.

Bound Structures of the MRLFV E-Peptide. By addition of 0.4 μM *S. aureus* ribosomes in the NMR sample containing 2 mM E-peptide in H_2O buffer solution, the NOE correlations with a mixing time of 150 ms become negative and their intensities increase. A total of 52 TRNOEs were interpreted from TRNOESY spectra at 150 ms. Of these, 33

Table 1: ^{1}H and ^{13}C Resonance Assignments for the E-Peptide (MRLFV) at 293 K[a]

	^{1}H assignments							^{13}C assignments				
residue	NH	αH	βH	γH	δH and others		ΔδNH = *f*(*T*)	αC	βC	γC	δC and others	
Met 1	*b*	3.82	2.01	2.56	εH	2.12		55.9	34.3	40.0	εC	17.1
Arg 2	*b*	4.32	1.73	1.53	δH	3.16		56.1	30.6	42.6	δC	43.0
Leu 3	8.36	4.34	1.42, 1.58	1.56	δ_AH	0.84	−8.5	55.3	26.9	26.6	δ_AC	23.0
					δ_BH	0.91					δ_BC	24.5
Phe 4	8.31	4.69	2.99, 3.20		^{2,6}H	7.28	−8.0	57.1	39.2		^{2,6}C	131.8
					^{4}H	7.31					^{4}C	129.4
					^{3,5}H	7.36					^{3,5}C	130.9
Val 5	7.67	4.04	2.07	0.88, 0.91			−7.0	63.1	34.3	19.8, 21.3		

[a] In 90% H_2O/10% D_2O buffer. [b] Exchanged with solvent.

Table 2: ^{1}H and ^{13}C Resonance Assignments for the K-Peptide (MRFFV) at 293 K[a]

	^{1}H assignments							^{13}C assignments				
residue	NH	αH	βH	γH	δH and others		ΔδNH = *f*(*T*)	αC	βC	γC	δC and others	
Met 1	*b*	3.81	1.95	2.43, 2.47	εH	2.07		55.8	34.7	31.6	εC	17.1
Arg 2	*b*	4.28	1.64	1.41, 1.49	δH	3.13		56.2	31.4	27.0	δC	43.6
Phe 3	8.28	4.61	2.90,		^{2,6}H	7.22	−10.0	57.5	40.2		^{2,6}C	132.1
			3.05		^{4}H	7.30					^{4}C	130.0
					^{3,5}H	7.34					^{3,5}C	131.6
Phe 4	8.28	4.68	2.97,		^{2,6}H	7.27	−7.0	57.6	40.2		^{2,6}C	132.2
			3.18		^{4}H	7.30					^{4}C	130.0
					^{3,5}H	7.35					^{3,5}C	131.6
Val 5	7.68	4.00	2.07	0.90, 0.92			−7.0	63.7	33.8	20.6,21.8		

[a] In 90% H_2O/10% D_2O buffer. [b] Exchanged with solvent.

were intraresidue interactions, 12 sequential ($|i - j| = 1$), and two nonsequential ($|i - j| = 2$) interresidue interactions (Figures 3A and 4A and Table 3 in the Supporting Information). We observed an increase in the observed NOE correlations compared to those from the spectra in aqueous buffer solution.

In the bound state, some characteristic cross correlations appeared, especially TRNOEs between L3 H_δ and H_β and the aromatic region of F4 $H_{\delta1,\delta2}$ and $H_{\epsilon1,\epsilon2}$ (Figure 3A). Using these correlations as distance restraints, simulated annealing experiments were performed for the bound E-peptide. The peptide MRLFV-bound structures (Figure 5) were generated with Φ and Ψ in the allowed regions of the Ramachandran plot (Figure 10 in the Supporting Information).

The L3 H_δ−F4 $H_{\delta1,\delta2}$, L3 H_δ−F4 $H_{\epsilon1,\epsilon2}$, and L3 H_β−F4 $H_{\delta1,\delta2}$ TRNOEs, characteristic of the bound E-peptide (MRLFV) state, induced a bent peptide backbone with a "folded down" F4 phenyl unit (Figure 5C). In the bound structures, the R2 side chain can take up two major positions: either the guanidyl unit was directed up perpendicular to the peptide backbone (**S1**), or it was folded down in a cyclic form (**S2**). The superimposition of the 20 best **S1** and **S2** structures is shown in panels A and B of Figure 5, respectively. The average rmsds over the set of 20 **S1** and **S2** structures for main chain atoms (N, C_α, and C) were 0.59 and 1.25 Å, respectively. The total energy of the **S2** structure containing the folded down Arg side chain is lower than the total energy of the **S1** structure with the linear side chain (84 and 90 kcal/mol, respectively), while the TRNOE energy is higher (1.4 and 0.2 kcal/mol, respectively). The electrostatic interactions between the R2 guanidyl unit and the V5 C-terminus carbonyl group stabilize the R2−V5 stacking in the **S2** structures. On the other hand, in **S1**, contacts of the R2 side chain with the V5 residue are nonexistent, and thus, there is a total release of this unit which is no longer maintained by stacking. Therefore, the bound structure of the E-peptide is characterized by a bent peptide backbone and by two possible positions of the Arg side chain.

Bound Structures of the K-Peptide (MRFFV). By addition of 0.4 μM *S. aureus* ribosomes to the NMR sample containing 2 mM K-peptide (MRFFV) in H_2O buffer solution, TRNOEs were used to determine the bound structure. Since the K-peptide is in fast exchange on the cross-relaxation time scale of the bound peptide, the observed TRNOESY intensities are sums of the bound and free peptide NOEs. In this study, analysis of TRNOEs was simplified since NOEs which were present for the free peptide were smaller than those for the bound state. With shorter mixing times (50 ms), free K-peptide NOEs represent at most 10% of the uncorrected NOEs because of the longer mixing times (600−800 ms) used in the free state analysis. Also, analysis of TRNOEs was simplified since the cross-relaxation rates of the K-peptide in the free ($\omega\tau_c < 1$) and bound state ($\omega\tau_c > 1$) are opposite in sign. A total of 87 NOE interactions were interpreted from TRNOESY spectra; 27 are sequential ($|i - j| = 1$) and 14 nonsequential interresidue interactions [12 ($i - i + 2$) and 2 ($i - i + 3$)] (Figures 3B and 4B and Table 4 in the Supporting Information).

In the bound state, some characteristic cross correlations appeared, especially interactions concerning the aromatic region of the two Phe residues (F3 and F4) with the other amino acids (M1, R2, and V5) (Figure 3B). V5 H_γ−F3,4 $H_{\delta,\epsilon}$, R2 H_β−F4 $H_{\delta,\epsilon}$, and M1 H_β−F3 $H_{\delta,\epsilon}$ TRNOEs (Figure 3B) are determinants for the conformation of the bound K-peptide. These TRNOE correlations induced only one folded down structure (**S3**) (Figure 6B). Simulated annealing experiments, using TRNOEs correlations as distance constraints, were performed on the K-peptide. The resulting bound structures were characterized by one major Φ−Ψ distribution (Figure 11 in the Supporting Information)

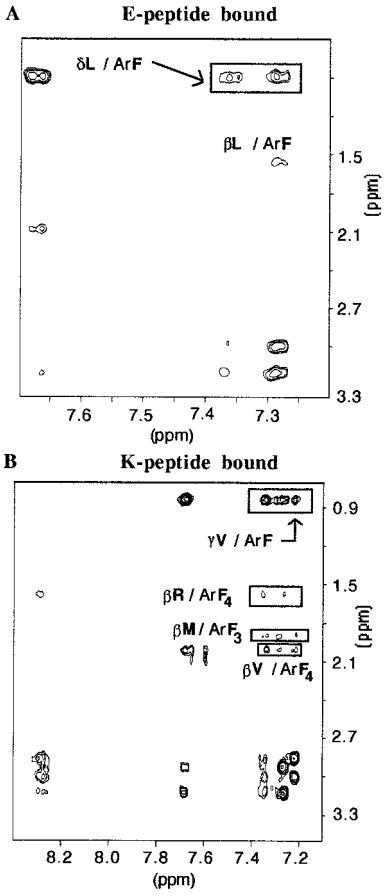

FIGURE 3: 2D [^{1}H,^{1}H] NOESY spectra (500 MHz) of the region containing amide and aromatic proton−aliphatic proton cross-peaks of the E- and K-peptides. (A) E-peptide (MRLFV) in H_2O buffer solution with 0.4 μM *S. aureus* ribosomes at 293 K. (B) K-peptide (MRFFV) in H_2O buffer solution with 0.4 μM *S. aureus* ribosomes at 293 K. The individual connectivities are boxed and identified with the one-letter amino acid code and the type of hydrogen atom. Note the presence of connectivities between the aromatic protons of K- and E-peptides in the bound state and the methyl groups of residues Val and Leu, respectively.

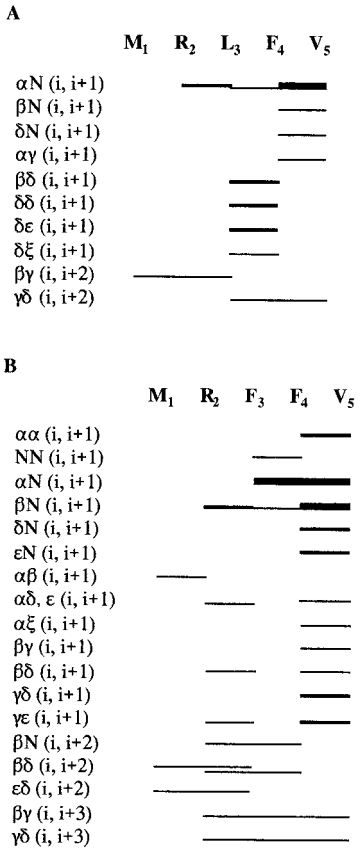

FIGURE 4: Sequential and medium-range NOE connectivities in the peptides. (A) E-Peptide (MRLFV) in H_2O buffer solution with 0.4 μM *S. aureus* ribosomes at 293 K. (B) K-Peptide (MRFFV) in H_2O buffer solution with 0.4 μM *S. aureus* ribosomes at 293 K. NOEs are arranged in terms of strong (thick lines), medium (medium lines), and weak (thin lines) intensities.

corresponding to the **S3** conformation (Figure 6A). Of 200 generated structures, 20 superimposed well with average backbone rmsd values of 0.38 Å (Figure 6A), and they illustrate the good stability of the bound K-peptide conformation. The total energy for the best structure was 129 kcal/mol and the TRNOE energy 4.9 kcal/mol. The qualitative interpretation of the TRNOE data is in agreement with the result of structure calculations. Again, as for the bound E-peptide, the K-peptide backbone adopts a "turn" structure (Figure 6B). It was noticed that the TRNOEs between the side chains of the bound K-peptide indicate their proximity in a relatively rigid orientation. The hydrophobic side chains are packed two at a time, so the tertiary structure of the bound K-peptide appears to be very compact.

The pattern of TRNOE connectivities for the bound K-peptide (87) compared to the spectra of the E-peptide (52) was indicative of a more rigid bound conformation. This suggests that in the receptor-bound state its conformation is "locked in", and thus, the K-peptide has a higher affinity. The differences between E- and K-peptide bound structures result from a lack of TRNOE-derived distance constraints in the E-peptide due to the high flexibility of the two Arg and Phe side chains. In the structure relevant to the K-peptide receptor binding conformation **S3**, the side chains of the two residues (R2 and F4) are involved in mutual interactions that suppress end fraying and thus stabilize the turn while the two major conformations of the E-peptide, **S1** and **S2** (less associated molecule with the receptor), do not present the same structural analogy of the side chains.

DISCUSSION

E- and K-Peptide Interaction on Ribosomes. Here also, TRNOE NMR experiments were proven to be efficient for the location and detection of the weak interactions due to ribosomal activity. Specific interactions of the E-peptide (MRLFV) and K-peptide (MRFFV) binding to their targets can be observed as a blank result was obtained in control experiments. It was clear from these data that the active resistance peptides bound weakly to bacterial ribosomes in a manner similar to that of macrolides or ketolides.

In this study, we have taken advantage of transferred nuclear Overhauser effects to gain information about the conformation of E- and K-peptides in the bound state and to compare their weak interaction responses. This allows us to investigate the structural properties responsible for the allosteric effects between antibiotics and peptides on the weak ribosomal binding site. Thus, in the ribosome complex, from the constraints of the different TRNOEs observed in buffer solution, we propose to analyze if the bound structures belonging to ketolide and macrolide resistance peptides

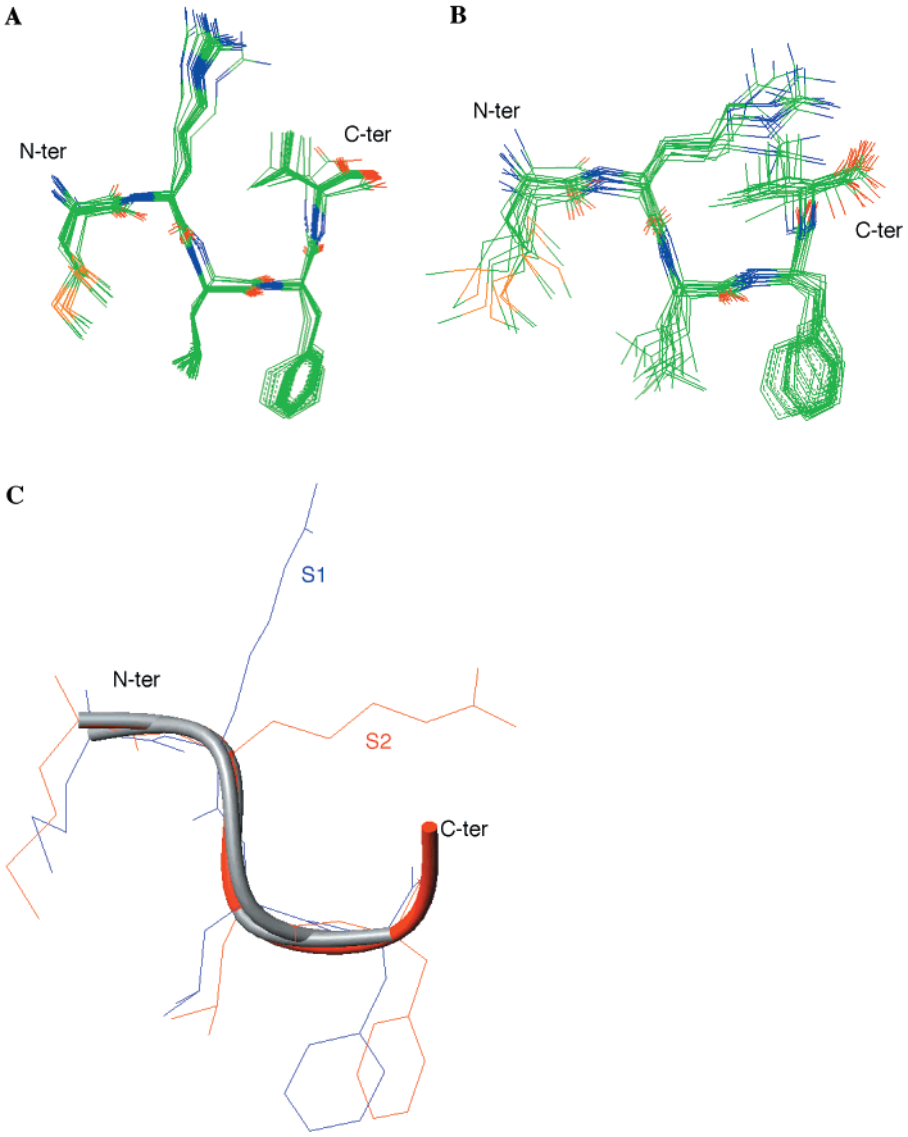

FIGURE 5: Structure of the E-peptide (MRLFV) bound to *S. aureus* ribosomes based on simulated annealing (SA) using the TRNOE data. (A) NMR-bound structure of the E-peptide with the smallest rmsd. Superimposition of the best 20 calculated bound structures (**S1**) that had low total energy and low TRNOE restraint energy yielded an rmsd of 0.59 Å. (B) Second ensemble of 20 calculated bound structures containing a folded down Arg side chain (**S2**), with an rmsd of 1.25 Å. (C) Comparison of the E-peptide backbones between the bound structure **S2** (red) and **S1** (gray) superimposed for the best fit. The figure was prepared with the program MOLMOL.

present a shared bound region. The superimposition of the bound E- and K-peptides gives great structural information (Figure 6C). In water, the absence of NOE correlations and the few weak ROE correlations probably reflect the intense hydration of the NH and CO sites, which prevents them from interacting in a defined backbone conformation. In the presence of *S. aureus* ribosomes, **S2** and **S3** conformations appear to be the plausible bound structures relative to the weak specific binding to the bacterial ribosomes. Figure 6C shows the backbone atom superimposition (rmsd = 0.28 Å) of the **S3** K-peptide and the **S2** E-peptide (with the folded down R2 side chain). The main peptide backbone appeared to clearly make a loop in the two structures. This could represent a nascent turn in the bound conformation, but it was not as well constrained by the NMR data in the E-peptide as in the K-peptide.

Comparison of E- and K-Peptide Interaction. When we added *S. aureus* ribosomes, the line widths of K-peptide signals were more broadened (about 3 times) than the line widths of E-peptide signals even at the same antibiotic/ribosome ratio. Moreover, for the K-peptide, maximum TRNOE cross-peaks occur at shorter mixing times than for the E-peptide. These facts indicate for the K-peptide a better affinity for the binding region than for the E-peptide. It was noticed that the ketolide telithromycin showed an higher affinity for the 70S ribosome target than did macrolides (*16*) and displayed a significantly better overall antibiotic activity.

A significant increase in K-peptide activity against antibiotics depends on many factors, and these may include the bound conformation. The bound state of the E-peptide is less rigid than the bound state of the K-peptide. The E-peptide backbone must adopt the structure with the folded down Arg chain stabilized by the R2−V5 stacking. In the K-peptide, the F4 aromatic chain is maintained by stacking with the guanidyl group of the R2 residue providing a particular hydrophobic and globular fragment (Figure 6C). The stacking of the aromatic and Arg side chain may be important for the antibiotic resistance peptide mode of action. The same local element has been observed with the imidazolyl−pyridine chain in the ketolide molecules where the introduc-

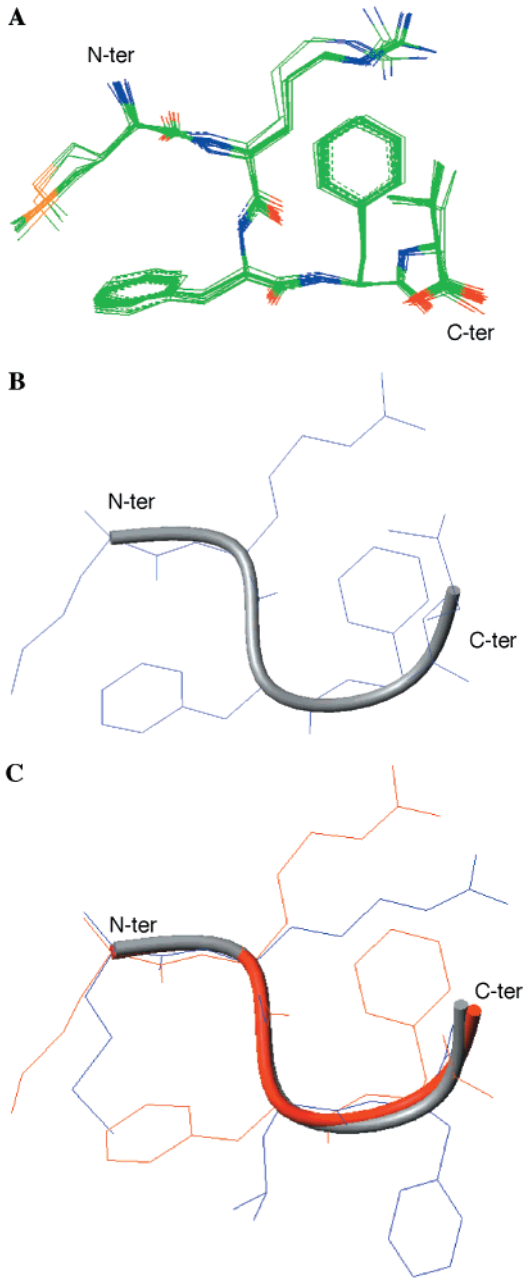

FIGURE 6: Conformation of the K-peptide (MRFFV) bound to *S. aureus* ribosomes. (A) Superimposition of the best 20 calculated structures generated by MD with distance constraints based of the observed TRNOE data, with an rmsd of 0.381 Å. (B) TRNOESY-derived structure **S3** of the K-peptide bound to bacterial ribosomes. (C) Superimposition of the structures representing the bound state of the antibiotic resistance peptides, **S2** (E-peptide) and **S3** (K-peptide) in red, in which the peptidyl backbone is almost completely superimposable (rmsd of 0.28 Å). Superimposition revealed one change in a side of the K-peptide molecule that may be important for the antibiotic resistance peptide mode of action, namely, the stacking of the aromatic and Arg side chain.

tion in ketolides of an aryl−alkyl side chain resulted in a significant increase in activity against resistant strains. Superimposition of the bound structures (Figure 7) revealed another change that may be important for the ketolide resistance peptide, namely, the proximity and the rigid orientation of the hydrophobic M1−F3 side chains found in the K-peptide. At the N-terminus, the side chains of M1 and F3 form a "clip motif" only in the K-peptide bound state, providing a change in hydrophobicity on the target site.

E- and K-Peptide Binding Surface. The most obvious evidence for ribosome−peptide interactions is the binding-induced differential line broadening in the NMR spectra of the peptides. In particular, the observed broadening may reflect proximity to a binding surface. Models of the E-peptide (MRLFV) and the K-peptide (MRFFV) showing the hydrogen atoms giving the most extensively broadened resonances were constructed using van der Waals surfaces (Figure 7). The "surface" of the peptides deduced from the variation in line broadening would be indicative of the relatively rigid part of the molecules. For both the E- and K-peptide, the Arg side chain was found to be essentially perpendicular to shut the turn. In the case of the E-peptide, the data corresponding to aromatic protons of F4 and aliphatic protons of the R2 regions (Figure 7A) are indicative of near-rigid rotation of these atoms in the proximity of the ribosome due to specific interunit (ribosome−peptide) bonds involving this region. The differential line broadening of the K-peptide is really similar to the E-peptide data, but a larger broadening was specifically observed in the R2 guanidyl and F4 phenyl groups of **S3**. A significant line broadening of the F3 phenyl unit indicates also a proximity of this residue in the K-peptide−ribosome complex. Figure 7B shows a hydrophobic cluster localized on the side of the aromatic cycle of the F4. Both E- and K-peptides bind to the bacterial ribosome, but perhaps in a different way. Evidence from the differential line broadening of peptide resonances suggested that the F4 side chain is probably in direct contact with the ribosome.

E- and K-Peptide in Competition with Antibiotics for Binding to the Ribosomes. The competitive effects between the E- and K-peptides and roxithromycin ketolide antibiotics give us some precious information about the mode of action of the pentapeptides and the topology of the ribosomal weak binding domain of antibiotics. The synthesized pentapeptides interact with the drug weak binding site and actively displace the antibiotic from the ribosome, but this competitive effect is not sufficient to explain the antibiotic resistance. Even if an allosteric effect was found for the weak ribosomal binding domain of macrolide and ketolide antibiotics, there was not a good specificity for the antibiotic's displacement. However, the ketolide is more efficiently displaced by the K-peptide than by the E-peptide. The resistance peptides and the macrolide (or ketolide) group compete for binding to the ribosomes, indicating the existence of overlapping sites of interaction. Exogenous E- and K-peptides are adapted to each type of binding site. Members of the erythromycin family apparently block protein synthesis only after the formation of several peptide bonds due to steric hindrance by the drug molecule. The specific endogenous short peptides have been translated on the ribosome, and they are able to interfere with the drug-binding site. Then the drug is probably displaced some distance along the exit route of the peptide chain formation.

Resistance Peptides: Mode of Action. The results of the specific interaction with the ribosomes and of the competitive effects reveal a new aspect of interaction of resistance peptides with ribosome and macrolide antibiotics. The bottle brush mode of action implicates direct interaction between the resistance peptides and macrolide or ketolide antibiotics on the ribosome (*28*). However, the detailed mechanism of such interaction remains obscure. Here, our experiments

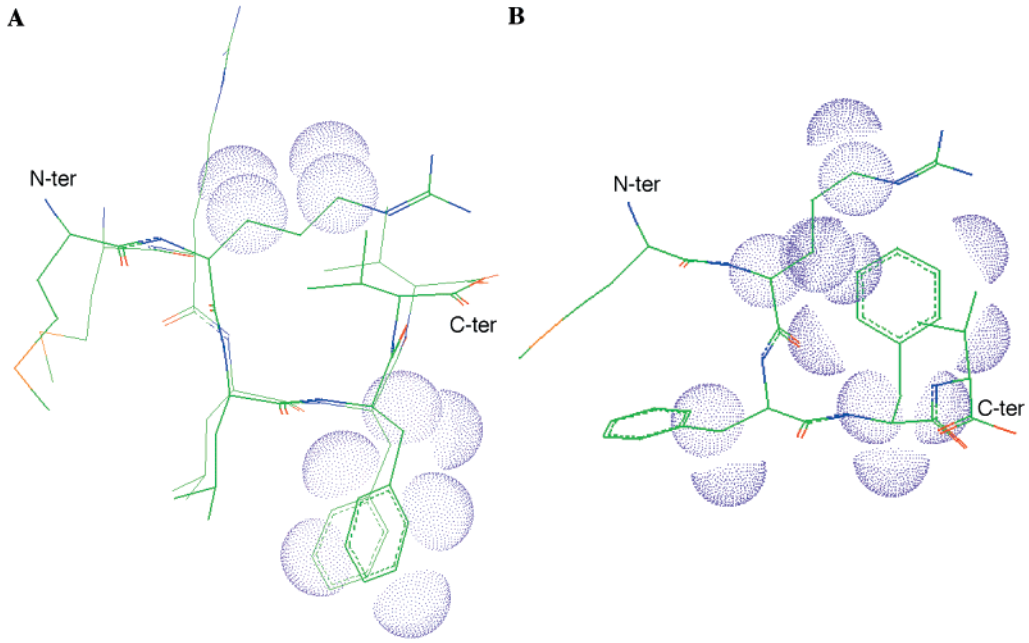

FIGURE 7: van der Waals surfaces are shown to indicate the atoms whose signals are broadened. The observed broadening may reflect the proximity to a binding surface. (A) δ Leu, φ Phe, γ Val, and β Arg in the structures of the E-peptide bound to ribosomes (the major one, in bold). (B) φ 3−4 Phe, γ Val, and β Arg in the structures of the K-peptide bound to ribosomes.

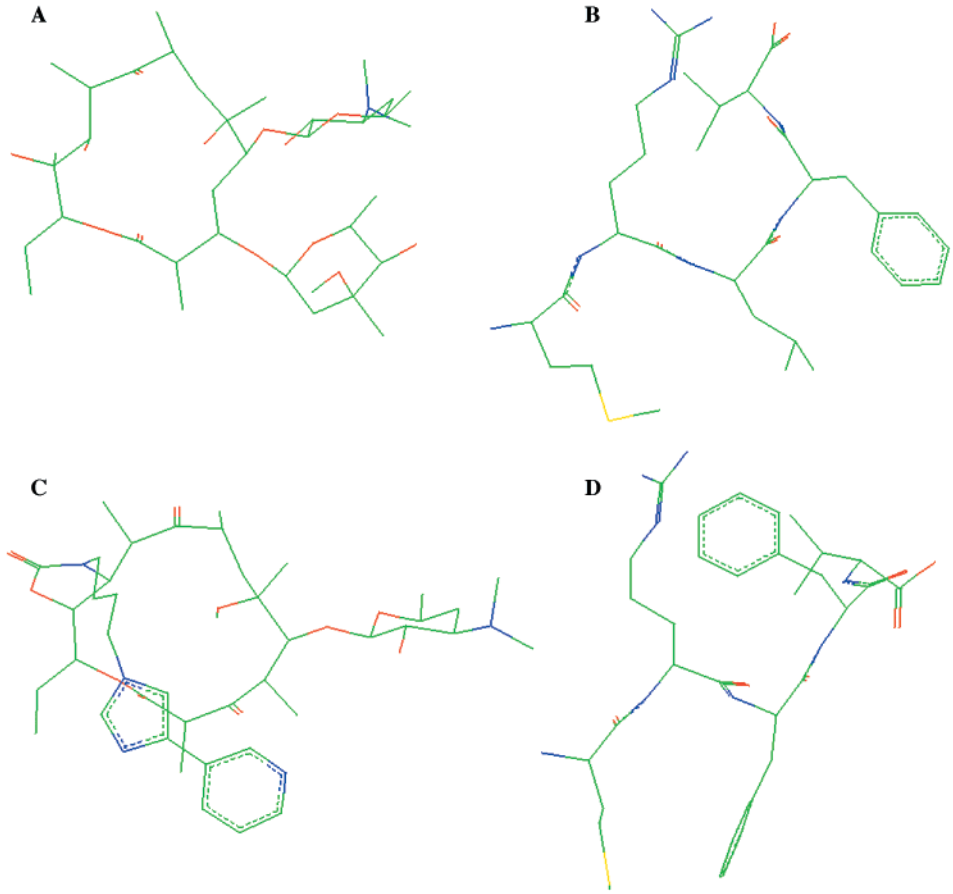

FIGURE 8: Comparison of structures of the E- and K-peptide bound to *S. aureus* ribosomes in competition with antibiotics erythromycin and telitromycin for binding to the ribosomes: (A) erythromycin-bound structure, (B) E-peptide-bound structure, (C) telitromycin-bound structure, and (D) K-peptide-bound structure.

suggest new insights about the mode of action of the endogenous resistance peptides. The resistance mechanism may probably imply two steps, a competitive effect of the resistance peptide for the macrolide (or ketolide) binding site followed by a bottle brush effect in which the drug and the peptide are driven out of their binding site, thus removing the antibiotic from the ribosome.

This mechanism is of significant interest since it answers some questions about the mode of action of the pentapeptides. (i) The length requirement for functional peptides was

five or six amino acids, suggesting that the small size of erythromycin resistance peptides was important in the mechanism of peptide action (*33*). In the ribosome complex, the associated molecules require a cyclic orientation of the peptide backbone similar to that found for the macrocycle of antibiotics (Figure 8). The size and the consensus sequence of the resistance peptide favor a particular hydrophobic and globular fragment, indicating that a similar type of interaction between the resistance peptide or antibiotics on the ribosome can occur in both cases. (ii) The amino acid sequence of the peptides is related to the type of macrolide antibiotic (*28*). The bottle brush model proposed by Mankin is based on this observation. However, specific binding of the peptide is also in agreement with the selective sequence of the peptides because the binding sites of each macrolide could have their own specificity. The aliphatic protons of R2 guanidyl in E- and K-peptides and aromatic protons of F4 phenyl regions (Figure 7A) are involved in the binding surface. These substituents favor hydrophobic interaction between antibiotic resistance peptides and the ribosome. The interaction between the weak binding domain of the ribosome and the peptides should be hydrophobic in part as it also has been supposed for the macrolide−ribosome weak interaction (*22*). The folded down structure of the bound peptides associated with the hydrophobic cluster shows similarities with the binding model of erythromycin and telithromycin (Figure 8). (iii) Mankin and co-workers have demonstrated that the pentapeptides affect the function of the ribosome in cis, and peptides were synthesized in the ribosome and traversed the nascent peptide channel from the inside to the outside. Exogenously added synthetic E-peptide was not effective in the cell-free translation system at physiological concentrations (*27*). Under our experimental conditions, we can observe the E-peptide binding to the ribosome when it comes from the outside because of the great excess of ligand (E-peptide/ribosome ratio of 5000) in an intermolecular process. The reaction mechanism could be analyzed and could account for kinetic data. It is important to distinguish the molecularity involved in the sequence of steps of the resistance reaction. The ribosome with the "not-released" endogenous E- or K-peptides corresponds to a single entity, and thus, in this unimolecular step, this complex shakes itself apart or shakes its atoms into a new arrangement. The number of "ribosome−peptide" molecules that react in a short interval is proportional to the number available to react, and so the rate of change of the amount of ribosome−peptide complex is proportional to its concentration. That is different from the competition reactions described in the current paper. Our results show that exogenously added synthetic E- or K-peptides could interact with a 70S ribosome and inhibit the macrolide weak binding site. In the bimolecular step in which the molecules collide and exchange energy or undergo some other kind of change (conformational), concentrations must be in large excess for a similar result. (iv) Expression of the pentapeptides renders the cell resistant to relatively low concentrations of antibiotics (*28*). The two-step mechanism described above could explain this fact. In such a mechanism, relatively low concentrations of drugs do not allow drugs to be effective competitors with respect to endogenous peptides. (v) The observed competitions of the peptides with the antibiotics on the ribosome exhibit similar K_D values. However, our results show a competitive effect as an intermolecular event (peptide and ribosome are independent), while the in vivo mode of action can be assumed to be intramolecular because the endogenous peptide is constrained naturally by the ribosome and localized near its binding site. Then the K_D value of the not-released cis peptide should be lower.

It is possible that some cases of erythromycin resistance observed in clinical isolates can be due to mutations in the rRNA genes activating expression of the E-peptide (*33*). Multiple examples of peptide sequences capable of conferring resistance to different macrolide antibiotics suggest that similar mechanisms of antibiotic resistance may potentially operate in nature and may account for macrolide resistance of some clinical pathogens. Antibiotic resistance peptide studies may provide insights into functionally important features of other cis-acting peptides and may eventually lead to a better understanding of how the macrolide antibiotics act upon the ribosome.

ACKNOWLEDGMENT

We are grateful to Prof. A. S. Mankin for helpful discussions.

SUPPORTING INFORMATION AVAILABLE

Tables of qualitative nuclear Overhauser enhancement data and observed TRNOEs for E- and K-peptides, respectively; figures of the variation of Φ and Ψ and total potential energy (E_n) during the simulated annealing period for the five residues of E- and K-peptides as a function of time for the whole 200 ps; and Ramachandran plots containing all residues and individual residue Ramachandran plots of NOE- and TRNOE-constrained structures for the E- and K-peptide. This material is available free of charge via the Internet at http://pubs.acs.org.

REFERENCES

1. Denis, A., Agouridas, C., Auger, J. M., Benedetti, Y., Bonnefoy, A., Bretin, F., Chantot, J. F., Dussarat, A., Fromentin, C., Goin D'Ambrières, S., Lachaud, S., Laurin, P., Le Martret, O., Loyau, V., Tessot, N., Pejac, J. M., and Perron, S. (1999) *Bioorg. Med. Chem. Lett. 9*, 3075−3080.
2. Agouridas, C., Colette, P., Mauvais, P., and Chantot, J. F. (1994) *34th Interscience Conference on Antimicrobial Agents and Chemotherapy*, F-166, American Society for Microbiology, Washington, DC.
3. Ednie, L. M., Spangler, S. K., Jacobs, M. R., and Appelbaum, P. C. (1997) *Antimicrob. Agents Chemother. 41*, 1033−1036.
4. Ednie, L. M., Spangler, S. K., Jacobs, M. R., and Appelbaum, P. C. (1997) *Antimicrob. Agents Chemother. 41*, 1037−1041.
5. Jamjiam, C., Biedenbach, D. J., and Jones, R. N. (1997) *Antimicrob. Agents Chemother. 41*, 454−459.
6. Agouridas, C., Bonnefoy, A., and Chantot, J. F. (1995) *35th Interscience Conference on Antimicrobial Agents and Chemotherapy*, F-158, American Society for Microbiology, Washington, DC.
7. Goldman, R. C., Fesik, S. W., and Doran, C. C. (1990) *Antimicrob. Agents Chemother. 34*, 426−431.
8. Fernandez-Munoz, R., and Vazquez, D. (1973) *J. Antibiot. 26*, 107−108.
9. Pestka, S. (1974) *Antimicrob. Agents Chemother. 6*, 474−478.
10. Agouridas, C., Benedetti, Y., Denis, A., Le Martret, O., and Chantot, J. F. (1995) *34th Interscience Conference on Antimicrobial Agents and Chemotherapy*, American Society for Microbiology, Washington, DC.
11. Agouridas, C., Benedetti, Y., Denis, A., Fromentin, C., Gouin d'Ambrières, S., Le Martret, O., and Chantot, J. F. (1994) *34th*

Interscience Conference on Antimicrobial Agents and Chemotherapy, F-164, American Society for Microbiology, Washington, DC.
12. Bertho, G., Gharbi-Benarous, J., Ladam, P., Delaforge, M., and Girault, J. P. (1998) *Bioorg. Med. Chem. 6*, 209−221.
13. Verdier, L., Gharbi-Benarous, J., Bertho, G., Evrard-Todeschi, N., Mauvais, P., and Girault, J.-P. (2000) *J. Chem. Soc., Perkin Trans. 2*, 2363−2371.
14. Barber, J., Gyi, J. I., and Pye, D. A. (1991) *J. Chem. Soc., Chem. Commun.*, 1249−1252.
15. Gyi, J. I., Brennan, R. J., Pye, D. A., and Barber, J. (1991) *J. Chem. Soc., Chem. Commun.*, 1471−1473.
16. Bertho, G., Gharbi-Benarous, J., Delaforge, M., Lang, C., Parent, A., and Girault, J. P. (1998) *J. Med. Chem. 41*, 3373−3386.
17. Gharbi-Benarous, J., Evrard-Todeschi, N., Ladam, P., Bertho, G., Delaforge, M., and Girault, J. P. (1999) *J. Chem. Soc., Perkin Trans. 2*, 529−543.
18. Bertho, G., Ladam, P., Gharbi-Benarous, J., Delaforge, M., and Girault, J. P. (1998) *Int. J. Biol. Macromol. 22*, 103−127.
19. Evrard-Todeschi, N., Gharbi-Benarous, J., Gaillet, C., Verdier, L., Bertho, G., Lang, C., Parent, A., and Girault, J. P. (2000) *Bioorg. Med. Chem. 8*, 1579−1597.
20. Agouridas, C., Denis, A., Auger, J. M., Benedetti, Y., Bonnefoy, A., Bretin, F., Chantot, J. F., Dussarat, A., Fromentin, C., Goin D'Ambrières, S., Lachaud, S., Laurin, P., Le Martret, O., Loyau, V., and Tessot, N. (1998) *J. Med. Chem. 41*, 4080−4100.
21. Verdier, L., Bertho, G., Gharbi-Benarous, J., and Girault, J.-P. (2000) *Bioorg. Med. Chem. 8*, 1225−1243.
22. Bertho, G., Ladam, P., Gharbi-Benarous, J., Delaforge, M., and Girault, J. P. (1998) *J. Chim. Phys. 95*, 423−429.
23. Dinos, G. P., and Kalpaxis, D. L. (2000) *Biochemistry 39*, 11621−11628.
24. Dinos, G. P., Michelinaki, M., and Kalpaxis, L. (2001) *Mol. Pharmacol. 59*, 1441−1445.
25. Neu, H. C. (1992) *Science 257*, 1064−1073.
26. Cohen, M. L. (1992) *Science 257*, 1050−1055.
27. Tenson, T., DeBlasio, A., and Mankin, A. (1996) *Proc. Natl. Acad. Sci. U.S.A. 93*, 5641−5646.
28. Tripathi, S., Kloss, P. S., and Mankin, A. (1998) *J. Biol. Chem. 273*, 20073−20077.
29. Vazquez, D. (1979) in *Inhibitors of Protein Synthesis*, pp 169−175, Springer-Verlag, Berlin.
30. Menninger, J. R., and Otto, D. D. (1982) *Antimicrob. Agents Chemother. 21*, 811−818.
31. Menninger, J. R. (1995) *J. Basic Clin. Physiol. Pharmacol. 6*, 229−247.
32. Dam, M., Douthwaite, S., Tenson, T., and Mankin, A. S. (1996) *J. Mol. Biol. 259*, 1−6.
33. Tenson, T., Xiong, L., Kloss, P., and Mankin, A. S. (1997) *J. Biol. Chem. 28*, 17425−17430.
34. Tenson, T., Herrera, J. V., Kloss, P., Guarneros, G., and Mankin, A. S. (1999) *J. Bacteriol. 181*, 1617−1622.
35. Dubois, B. W., and Evers, A. S. (1992) *Biochemistry 31*, 7069−7076.
36. Fraenkel, Y., Navon, G., Aronheim, A., and Gershoni, J. M. (1990) *Biochemistry 29*, 2617−2622.
37. Tsuchiya, M., Suzukake, K., Hori, M., Sawa, T., and Umejawa, H. (1981) *J. Antibiot. 24*, 305−312.
38. Swenden, C. L., and Johnson, W. (1976) *Infect. Immun. 14*, 345−354.
39. Piotto, M., Saudek, V., and Sklenar, V. (1992) *J. Biomol. NMR 2*, 661−665.
40. Rance, M., Sorensen, O., Bodenhausen, G., Wagner, G., Ernst, R. R., and Wüthrich, K. (1983) *Biochem. Biophys. Res. Commun. 117*, 479.
41. Hurd, R. E., and John, B. K. (1991) *J. Magn. Reson. 91*, 648−653.
42. Schleucher, J., Schwendinger, M., Sattler, M., Schmidt, P., Schedletzky, O., Glaser, S. J., Sorensen, O. W., and Griesinger, C. (1994) *J. Biomol. NMR 4*, 301−306.
43. Clore, G. M., and Gronenborn, A. M. (1982) *J. Magn. Reson. 48*, 402−417.
44. Clore, G. M., and Gronenborn, A. M. (1983) *J. Magn. Reson. 53*, 423−442.
45. Meiboom, S., and Gill, D. (1958) *Rev. Sci. Instrum. 29*, 688−691.
46. Ni, F. (1994) *Prog. Nucl. Magn. Reson. Spectrosc. 26*, 517−606.
47. Davis, D. G., Perlman, M. E., and London, R. E. (1994) *J. Magn. Reson., Ser. B 104*, 266−275.
48. Dauber-Osguthorpe, P., Roberts, V. A., Osguthorpe, D. J., Wolff, J., Genest, M., and Hagler, A. T. (1988) *Proteins: Struct., Funct., Genet. 4*, 31−47.
49. Nirmala, N. R., Lippens, G. M., and Hallenga, K. (1992) *J. Magn. Reson. 100*, 25−42.
50. Lanir, A., and Navon, G. (1971) *Biochemistry 10*, 1024−1032.

BI011319E